Computational modeling of polymer and carbon fiber composite interfaces

Mohammad Atif Faiz Afzal[a], Andrea R. Browning[a], Jeffrey Sanders[b], Thomas J. Mustard[a], Mathew D. Halls[c]

[a] Schrödinger, Inc., Portland, OR 97204, United States
[b] Schrödinger, Inc., New York, NY 10036, United States
[c] Schrödinger, Inc., San Diego, CA 92121, United States

Abstract

Carbon fiber composites are attractive materials in numerous applications, especially in the aerospace and automotive industries, due to their enhanced properties. More specifically, reinforcing polymeric materials with carbon fiber results in the increase of mechanical properties such as high elastic modulus. The interface between polymers and carbon fibers is a major part of the overall system and may play a role in the overall behavior. Studying the interactions between the graphite layers and polymers at the atomic scale will allow us to uncover insights that are not feasible via empirical observation. We have developed efficient molecular modeling methodologies to study these interactions and to evaluate the mechanical properties to quantify the enhancement in properties. We give examples using both thermoset and thermoplastic polymers. In the case of thermoset polymers, we provide details on the building the system and in-situ cross-linking. Additionally, we compare the interactions when the graphite sheets are aligned parallel and perpendicular to the polymer interface. The impact of the graphite layers on the crosslinking of thermosets is also discussed. In addition to the interface interactions, we study the stress-strain behavior of these composites and evaluate their modulus and yield point. Furthermore, we compare the location of void formation during the straining of the composite.

1. Introduction

The use of composite materials in the aircraft industry was initiated in the late 1960s after the development of carbon fiber manufacturing in 1964 at the Royal Aircraft Establishment at Farnborough, UK [1]. Since then, composite materials have replaced conventional materials, such as aluminum and titanium alloys, for primary aircraft structures. Carbon fiber reinforced polymer composites are known to have superior mechanical properties, such as high strength, fatigue resistance, high rigidity and high modulus [2-4]. In addition to mechanical properties, over the years, it is shown that composite materials have various other attractive properties such as flame and corrosion resistance [5, 6]. Furthermore, carbon fiber composite materials can be formulated as non-poisonous and bioinert [7]. Due to these appealing attributes, composite materials are extensively being used in automotive materials, defense and high-performance athletics equipment.

The carbon fiber structure consists of stacked graphene layers, where the layers are connected *via* van der Waals forces and within each layer the carbons are connected *via* strong covalent bonds [8]. This arrangement of layers results in high anisotropy in the carbon fiber structure. For example, the elastic

modulus along the direction parallel to the graphene layers is ~30 times more than the elastic modulus in the direction perpendicular to the layers [9]. An inverse effect is observed at the interface between the carbon fiber and polymer, i.e., strong adhesion is found at the polymer-graphite interface where the graphene sheet is parallel to the interface and a weak interaction when the sheet is oriented perpendicular to the interface [10-12]. Molecular modeling of the interface between polyethylene and graphene demonstrated that the interaction forces at the polymer-graphene interface is stronger than the interactions between the polymer chains [13]. Thermoset-graphite composite also demonstrate a similar behavior: Void formation under strain is nucleated in the thermoset bulk when the graphite is oriented parallel to the interface, whereas the void is initiated at the interface when the graphite is oriented perpendicular to the interface [10].

However, studies of such interactions for other thermoset and thermoplastic polymers are limited. We require further studies to confirm if the above-discussed behavior is a general trend in both class of polymers. We, therefore, perform atomistic simulations for polymer composites and give examples using both thermoset and thermoplastic polymers. We compute surface interaction energy at different orientations of graphite layers to quantify the adhesion behavior. Additionally, we perform stress-strain analysis and compare the mechanical properties of composites. We perform free volume analysis at various stages of straining to visualize the nucleation of void formation and compare the results for both orientations of graphite layers.

In addition to property calculation and analysis, we demonstrate the applicability and ease-of-use of Schrödinger's Materials Science Suite (MSS) tools to build and simulate polymer composite systems [14]. In the case of thermoset polymers, an additional step of crosslinking is required to build a statistically relevant network architecture. We have developed a comprehensive and easy-to-use crosslinking tool that is chemically agnostic; allowing users to activate diverse reactive chemistries. These tools take into consideration the reaction kinetics, obtained from our quantum mechanics (QM) tools, that are involved in the crosslinking step.

2. Methods

Molecular dynamics (MD) simulations serve as an economical alternative to lengthy experiments to study the thermal and mechanical properties of materials. In addition to property evaluation, MD can provide insights into the structure-property relationships that are otherwise not accessible empirically. For example, in the case of polymer composites, we can obtain insight into the interactions between polymer and graphite, and understand the mechanism of structural deformation under strain.

In this work, we implement polymer building tools and automated MD workflows, that are included in MSS, to build polymer systems and compute the mechanical properties, respectively [14]. We build four polymers: polystyrene (PS), poly(methyl methacrylate) (PMMA), poly(diglycidyl ether of bisphenol A) (PDGEBA), and poly(bisphenol A carbonate) (PBAC), and one crosslinked network of diglycidyl ether of bisphenol A (DGEBA) and 3,3' diamino-diphenyl sulfone (33DDS) (see Figure 1).

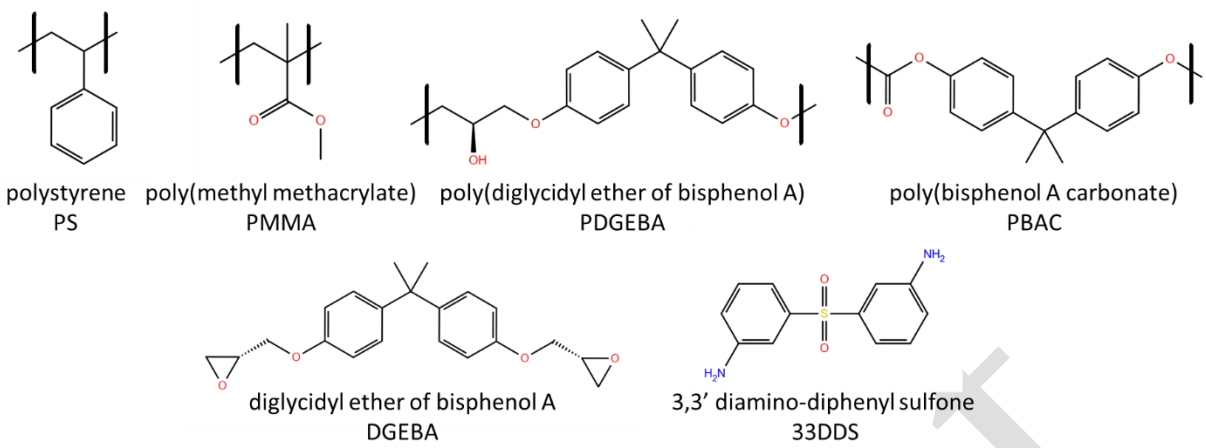

Figure 1: List of polymers and thermoset monomers studied in this work.

Polymer and disordered system builder

We build the PS, PMMA, PDGEBA, and PBAC chains using the Polymer Builder tool in MSS, which is a comprehensive tool for building homopolymers, block copolymers, and random copolymers. MSS version 19-1 is used for all build and simulations of this study. The polymer building workflow comprises of the drawing of a monomer structure, specifying the head and tail, and selecting the number of monomers. Example of the PDGEBA monomer and polymer structure is shown in Figure 2a and Figure 2b, respectively. For PMMA and PS, we build a chain with 100 monomer units, whereas for PDGEBA and PBAC, we build a chain of 50 monomer units.

Our process includes the creation of graphite layers and subsequently using these layers as a substrate to add polymer chains on the top. We create both parallel (PRL) and perpendicular (PPD) oriented graphite layers (see Figure 2c) using the Nanostructure Builder in MSS. We use Disordered System Builder in MSS to add amorphous polymer chains on top of graphite with a density of 0.8 g/cm3 (see Figure 2d). We select the number of polymer chains such that the final simulation box contains 20,000-25,000 atoms. We equilibrate these composite structures *via* a equilibration protocol that uses GPU accelerated Desmond MD engine and implements OPLS3 forcefield [4, 15]. For each polymer-graphite system, we create 10 replicates by changing the random seed in the Disordered System Builder panel.

We equilibrate the output structures from the Disordered System Builder using the MD Multistage Workflow tool in MSS. The equilibration procedure consists of four steps: the first step is Brownian Dynamics at constant volume and temperature (NVT) at 10 K for 20ps, the second step is Brownian Dynamics at constant pressure and temperature (NPT) at 100K for 20 ps, the third step is NPT at 300K/1atm for 100ps, and the fourth step is 110 ns NPT at 300K/1atm. The final equilibrated structure of PDGEBA-graphite composite system is shown in Figure 2e. We cast the output structures from this equilibration protocol into our property prediction workflows to evaluate the mechanical properties.

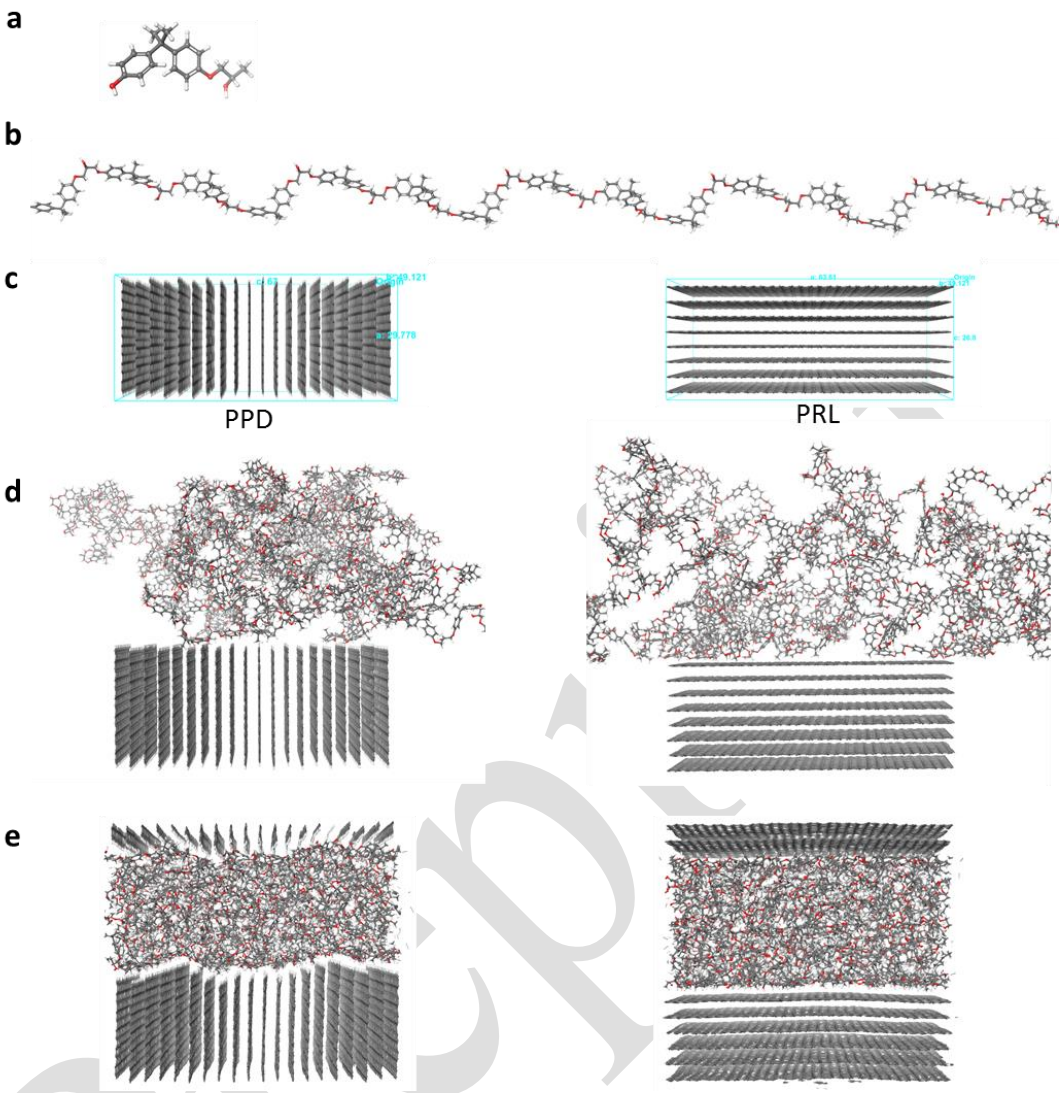

Figure 2: Typical workflow to create a polymer-composite simulation box in Schrödinger MSS. (a) DGEBA monomer structure; (b) DGEBA polymer structure; (c) graphite structure for PPD and PRL orientations, respectively; (d) disordered system of PDGEBA chains (unwrapped) on top of PPD and PRL graphite, respectively; (e) simulation box after final equilibration step at 300K for PPD and PRL configurations, respectively .

Crosslinking protocol

We use the crosslinking tool in MSS to create the simulation box of DGEBA-33DDS thermoset as described in ref. [16]. Before performing the crosslinking process, we add 250 and 125 molecules of DGEBA and 33DDS, respectively, on top of PRL and PPD graphite systems using the Disordered System Builder tool. We subsequently equilibrate the cell using the same procedure described earlier. We use the final equilibrated structure to perform crosslinking. The reaction scheme in the crosslinking procedure of DGEBA-33DDS system is shown in Figure 3. The primary amines and the secondary amines of 33DDS will have different reaction rates towards the epoxy group. We use QM and automated reaction workflow tools that are available in MSS to compute the reaction barriers for these reactions [17]. The reaction barriers for the primary amine and the secondary amine is calculated 39.3 kcal/mol and 31.5 kcal/mol, respectively. We use B3LYP-D3/6-31G** chemistry for geometry optimization and for energy calculation. We input the

reactions (using SMARTS pattern) and corresponding reaction barrier values in the crosslinking protocol to generate a realistic thermoset of DGEBA-33DDS system. We perform the crosslinking process until 90% of the epoxide groups are consumed. This total conversion is less than what is observed in experiments but was utilized in this study to more closely match thermoplastic systems. Higher conversions can be reached with extended crosslinking simulations. We limit the number of crosslinks to 40 per iteration. Each crosslinking iteration is followed by a 50ps NPT simulation at 800K/1 atm. A similar crosslinking protocol using MSS was previously demonstrated on other thermosets, such as benzoxazines and cyanate esters [18, 19]. A schematic of simulation cells at different stages of the above process is shown in Figure 4.

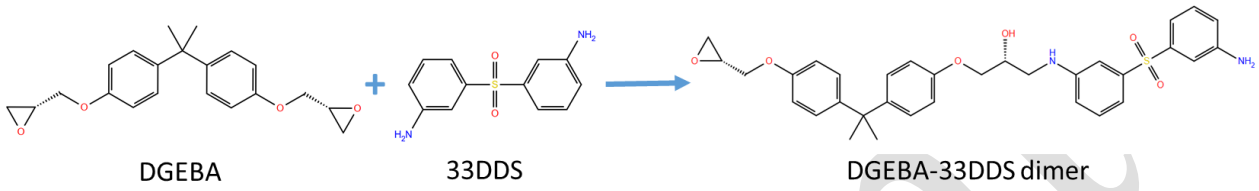

Figure 3: Reaction scheme in the crosslinking of DGEBA/33DDS thermoset system.

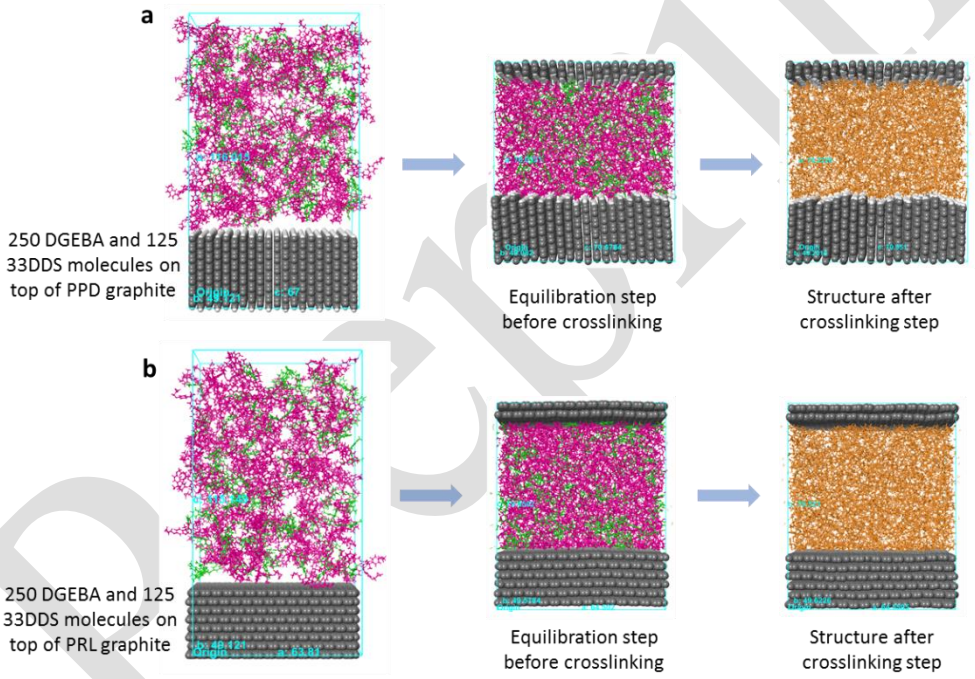

Figure 4: Schematic for obtaining a crosslinked simulation cell in MSS: (a) in PPD configuration, (b) in PRL configuration. The pink and green molecules represent DGEBA and 33DDS molecules, respectively. The orange structure represents crosslinked network.

Mechanical properties

We use the equilibrated polymer-graphite composite systems to compute their mechanical properties, in particular the elastic modulus, yield point and yield strain, using the Stress-Strain tool in MSS. The protocol for stress-strain calculation mimics the process of straining in one direction while simultaneously tracking the changes in the stress. We apply a pure uniaxial force with η=0, i.e., we keep the lateral dimensions constant while applying strain. The strain step size and the total number of steps are 0.1% and 200, respectively, resulting in a total of 20% strain. The simulation time for each straining step is set as 200ps

with a time step of 2fs. We perform all the stress-strain simulations at 300K. In both PPD and PRL orientations, we apply strain in the direction perpendicular to the polymer/graphite interface. For the evaluation of elastic modulus, yield point and yield strain, we average the stress-strain values for all the 10 replicates. Elastic modulus is calculated by taking the initial slope of the average curve. We consider first ten points (up to 1% strain) of the curve. The yield point and yield strain of the composite correspond to the point where highest stress is observed. In addition to these quantifications, we compute the free volume at different strain points to understand the nucleation of voids. We implement Free Volume tool in MSS, and use a probe radius of 1.4 Å and grid spacing of 0.25 Å to 1 Å with a step size of 0.25 Å.

3. Results

Mechanical properties

Figure 5 shows the stress-strain plots for PS, PMMA, PDGEBA, and PBAC polymer composites along both PPD and PRL orientation of graphite layers. The red and blue curves correspond to PRL and PPD orientation, respectively, and the shaded area represents the standard deviation across 10 replicates. For all the polymers, we observe that the behavior in the elastic region is similar for PRL and PPD configurations. The impact of graphite is more pronounced near the yield point, where we see that the proportional limit is longer in the case of PRL configuration. The yield point is higher in the PPD [1]orientation, but the difference is minor in the case of PDGEBA and PBAC.

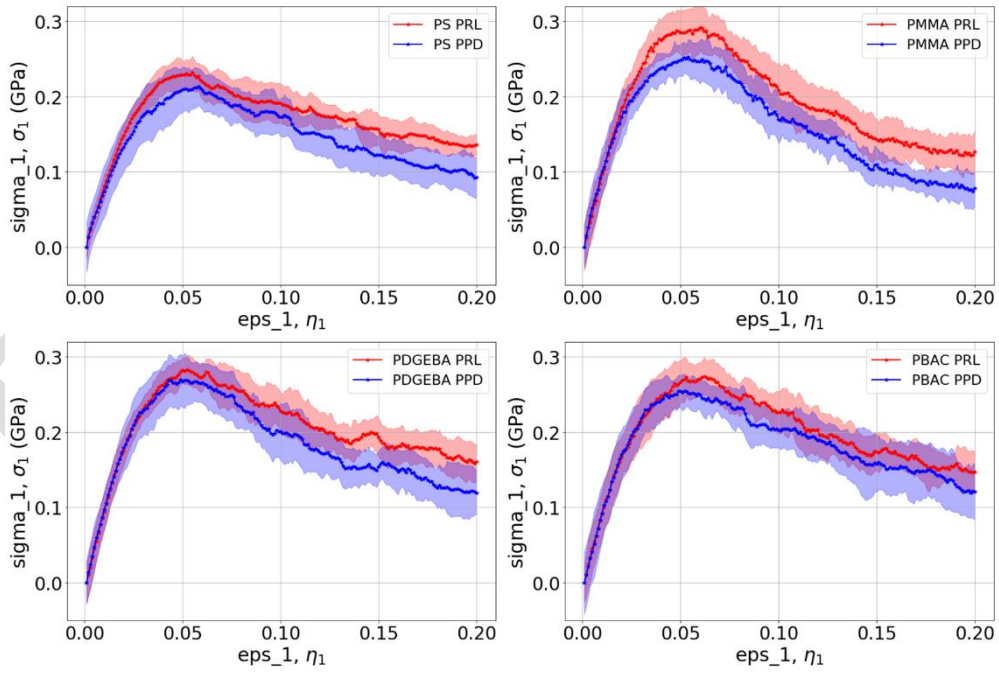

Figure 5: Stress-strain plots of PS, PMMA, PDGEBA, and PBAC in PRL and PPD configurations.

Table 1 shows the elastic modulus, yield point and yield strain of all the polymer composites. Comparing within PRL orientation, elastic modulus of PDGEBA (11.06 GPa) is the highest, followed by PMMA (10.32), PMMA (10.31 GPa), and PS (8.39 GPa). Except for PS, all the other polymers demonstrate comparable elastic modulus for PRL and PPD configuration. For PS, we see a drop of 0.8 GPa in elastic modulus when we go from PRL to PPD. It should be noted that the absolute value of modulus is impacted

by the rate of strain and lateral strain. The rate of current simulation strain (5 x 10^7 1/sec) loading is significantly higher than experiment (O(10^3) 1/sec), thus increasing the observed modulus and yield point. Keeping the lateral dimensions constant prevents Poisson's relaxation, which further increases observed modulus and yield point. Graphite orientation also impacts the yield point of the composite: for all other polymer-graphite systems, the yield point is higher in the case of PRL orientation. The most impact for thermoplastics is seen for PMMA where we observe a drop in the yield point from 0.29 GPa to 0.25 GPa. Within PRL orientation of thermoplastics, PMMA has the highest yield point followed by PDGEBA, PBAC, and PS. For yield strain, except for PS, we see a drop in the yield strain. In the case of DGEBA-33DDS crosslinked system, we observe a similar behavior, i.e, the elastic modulus is similar for PRL and PPD whereas the yield point and yield strain are both higher for PRL.

Table 1: Comparison of mechanical properties of polymer-graphite composites.

Polymer	Graphite orientation	Elastic modulus (GPa)	Yield strain	Yield point (GPa)
PS	PRL	8.39	0.055	0.228
PS	PPD	7.59	0.058	0.213
PMMA	PRL	10.32	0.060	0.292
PMMA	PPD	10.39	0.054	0.252
PDGEBA	PRL	11.06	0.053	0.283
PDGEBA	PPD	10.82	0.049	0.269
PBAC	PRL	10.31	0.063	0.272
PBAC	PPD	10.13	0.053	0.255
DGEBA-33DDS	PRL	12.14	0.068	0.36
DGEBA-33DDS	PPD	12.72	0.051	0.32

Void nucleation and free volume analysis

We track the trajectory of the stress-strain simulations to visualize the formation of void during the straining process. Figure 6a shows the snapshots of trajectory for PS (green), PMMA (blue), PDGEBA, (red) and PBAC (yellow) polymer composites with PRL orientation at total strain (η) of η = 0 and 0.2. In all these polymer composites with PRL graphite, we observe the location of void in the bulk of the polymer. This suggests that the interaction of the polymer with the graphite layers in PRL orientation is stronger than the interactions between polymer chains. Figure 6b shows the snapshots of the polymer composites with PPD orientation. In this case, the void nucleation occurs at the polymer/graphite interface as well as in the bulk of the polymer. A close look at the 3D structure of all the replicates suggests that the void nucleation during the straining in PPD configuration is predominantly at the interface. To obtain a better understanding of the void formation, we visualize the results from the free volume analysis. Figure 7 shows the free volume development with strain for PBAC composite. In the case of PPD orientation (see Figure 7a), void nucleation occurs at the interface as well as in the bulk of the polymer. At 20% strain, a significant portion of the void is at the interface as seen on top and bottom of graphite in the figure. For PRL orientation (see Figure 7a), almost all the voids are in the bulk of the polymer with no impact on the interface.

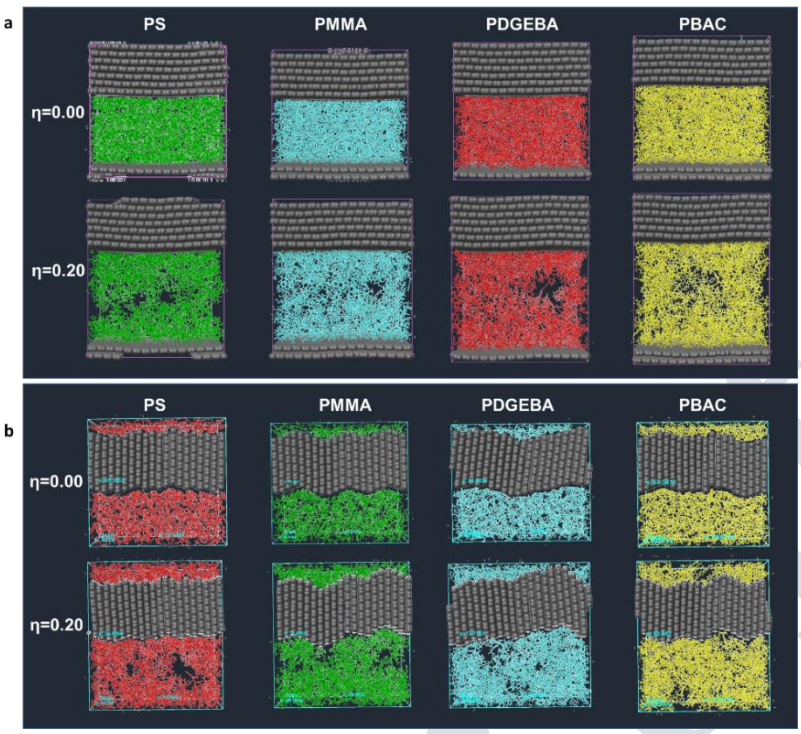

Figure 6: Snapshots from the trajectory of stress-strain simulations of PS, PMMA, PDGEBA, and PBAC: (a) for PRL configuration; (b) for PPD configuration.

Interaction energy

Table 2 shows the vdW, electrostatic, and total interaction energy values for the interaction between polymer and graphite. In all the cases, i.e. for all the polymers and all the type of interactions, the interaction energies in PPD configuration is lower than PRL configuration. This further corroborates our previous results that the interaction of polymer chains with the PRL graphite is significantly stronger than the interaction with PPD graphite. Electrostatic interaction shows PRL graphite is attractive for all polymers. Whereas the PPD graphite is attractive for PMMA and repulsive for PS, PDGEBA, and PBAC. Dispersive (vdW) is the major interaction for these polymer composite systems. The interaction is attractive in both orientations, but PPD graphite shows significantly less interaction with the polymer in comparison to PRL graphite. We observe similar trend in the interaction energies, a strong interaction at PRL interface compared to PPD, for the DGEBA-33DDS crosslinked system.

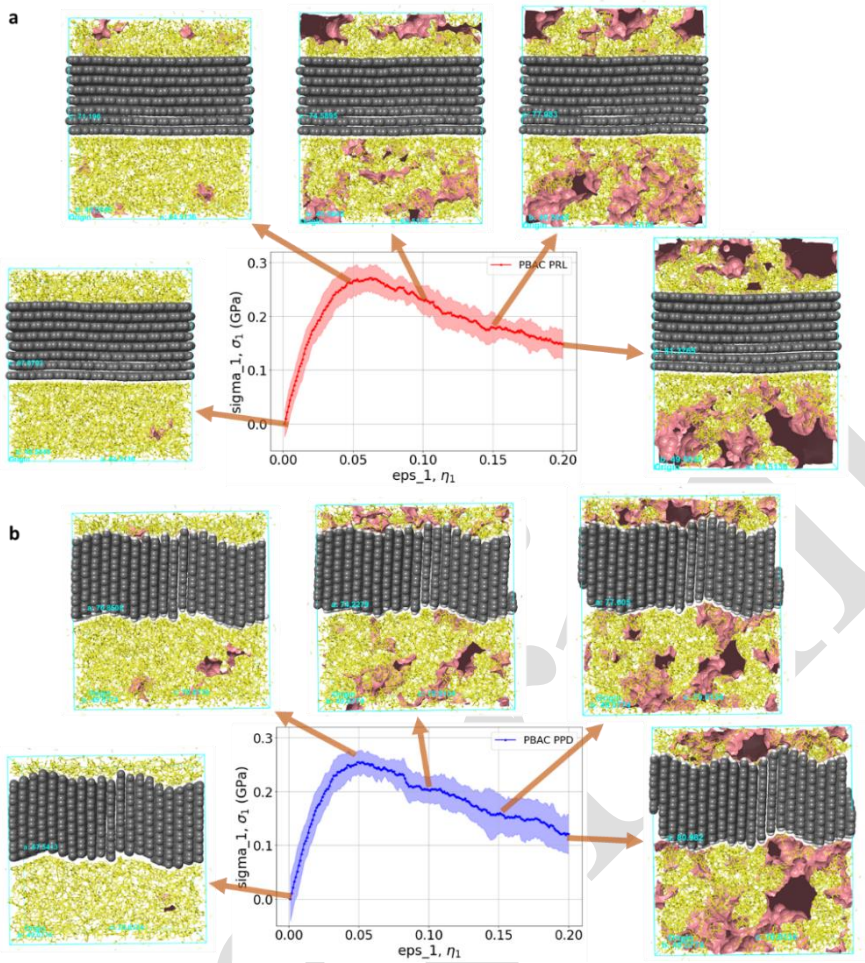

Figure 7: Free volume(solid blobs) at different strains during the stress-strain simulation of PBAC-graphite composite: (a) for PRL configuration; (b) for PPD configuration.

4. Conclusion

In this work, we demonstrated the applicability of MSS tools to efficiently and economically study the properties of polymer-graphite composites. We successfully created thermoplastic and thermoset composites with carbon fibers in both parallel and perpendicular orientations. We successfully demonstrated the application of QM and MD capabilities in MSS to generate realistic thermoset polymer systems. Mechanical property analysis showed superior attributes for composites with the parallel orientation of graphite. One of the limitations of our model is performing stress-strain simulations with very high straining rate, 5 x 10^7 1/sec, whereas the experiment rate is in the order of 10^3 1/sec. The high straining rate impacts the absolute value of the modulus and yield strength. Despite the large calculated values, our approach is highly efficient in reproducing the trends in the mechanical properties and aid in ranking materials. In addition to mechanical properties, we obtained unique insights into the polymer/graphite interactions and their interfacial behavior, which is extremely difficult to study empirically. Void nucleation during straining is observed in the bulk of the polymer when the graphite is oriented parallel to the

interface, whereas, the voids nucleate at the interface when graphite is perpendicular to the interface. Interaction energy analysis confirmed that the adhesion of polymer and graphite is significantly stronger in the parallel orientation. We successfully demonstrated that our computational approach is accurate in the evaluation of the mechanical properties of carbon fiber reinforced polymer composites. In subsequent work, we will utilize this modeling technique to characterize new thermoset and thermoplastic polymers and evaluate the impact of reinforcing such polymers with graphite.

Table 2: Interaction energy values for the interaction between polymer and graphite. The values are normalized by the interface area.

Polymer	Graphite orientation	vdW interaction energy (kcal/mol/Å^2)	Electrostatic interaction energy (kcal/mol/Å^2)	Total interaction energy (kcal/mol/Å^2)
PS	PRL	-43.55 ± 0.8	-0.16 ± 0.03	-43.71 ± 0.8
PS	PPD	-27.23 ± 0.69	3.94 ± 0.13	-23.29 ± 0.58
PMMA	PRL	-40.2 ± 0.9	-0.33 ± 0.04	-40.53 ± 0.91
PMMA	PPD	-25.33 ± 0.55	-0.24 ± 0.14	-25.57 ± 0.59
PDGEBA	PRL	-47.76 ± 0.59	-0.24 ± 0.03	-48 ± 0.57
PDGEBA	PPD	-31.1 ± 0.76	1.54 ± 0.14	-29.56 ± 0.77
PBAC	PRL	-50.54 ± 0.39	-0.20 ± 0.04	-50.74 ± 0.38
PBAC	PPD	-33.71 ± 0.67	1.62 ± 0.20	-32.09 ± 0.76
DGEBA-33DDS	PRL	-50.47 ± 0.66	-0.33 ± 0.06	-50.81 ± 0.66
DGEBA-33DDS	PPD	-33.07 ± 0.38	1.33 ± 0.16	-31.64 ± 0.44

References

1. Soutis, C., *Carbon fiber reinforced plastics in aircraft construction.* Materials Science and Engineering: A, 2005. **412**(1-2): p. 171-176.
2. Yasmin, A. and I.M. Daniel, *Mechanical and thermal properties of graphite platelet/epoxy composites.* Polymer, 2004. **45**(24): p. 8211-8219.
3. Sengupta, R., et al., *A review on the mechanical and electrical properties of graphite and modified graphite reinforced polymer composites.* Progress in Polymer Science, 2011. **36**(5): p. 638-670.
4. Stankovich, S., et al., *Graphene-based composite materials.* Nature, 2006. **442**(7100): p. 282-286.
5. Celzard, A., et al., *Conduction mechanisms in some graphite - polymer composites: the effect of a direct-current electric field.* 1997. **9**(10): p. 2225-2237.
6. Bian, X.-C., et al., *Dependence of flame-retardant properties on density of expandable graphite filled rigid polyurethane foam.* 2007. **104**(5): p. 3347-3355.

7. Björk, N., K. Ekstrand, and I.E. Ruyter, *Implant-fixed, dental bridges from carbon/graphite fibre reinforced poly (methyl methacrylate).* Biomaterials, 1986. **7**(1): p. 73-75.
8. Hull, D., et al., *An Introduction to Composite Materials*. 1996: Cambridge University Press.
9. Price, R.J., *Young's modulus of pyrolytic carbon in relation to preferred orientation.* The Philosophical Magazine: A Journal of Theoretical Experimental and Applied Physics, 1965. **12**(117): p. 561-571.
10. Li, C., et al., *Atomistic simulations on multilayer graphene reinforced epoxy composites.* Composites Part A: Applied Science and Manufacturing, 2012. **43**(8): p. 1293-1300.
11. Henry, D.J., et al., *Theoretical study of adhesion between graphite, polyester and silica surfaces.* Molecular Simulation, 2005. **31**(6-7): p. 449-455.
12. Yiapanis, G., et al., *Effect of Aging on Interfacial Adhesion between Polyester and Carbon-Based Particles: A Classical Molecular Dynamics Study*. 2007. **111**(17): p. 6465-6472.
13. Awasthi, A.P., D.C. Lagoudas, and D.C. Hammerand, *Modeling of graphene–polymer interfacial mechanical behavior using molecular dynamics*. Modelling and Simulation in Materials Science and Engineering, 2008. **17**(1): p. 015002.
14. *Materials Science Suite*. 2018, Schrödinger, LLC: New York, NY.
15. Harder, E., et al., *OPLS3: A Force Field Providing Broad Coverage of Drug-like Small Molecules and Proteins.* Journal of Chemical Theory and Computation, 2016. **12**(1): p. 281-296.
16. Sanders, J.M., et al. *Modeling Thermoset Polymers at the Atomic Scale: Prediction of Network Topology, Glass Transition Temperature and Mechanical Properties*. in *SAMPE* 2017. Seattle, WA.
17. Bochevarov, A.D., et al., *Jaguar: a high‐performance quantum chemistry software program with strengths in life and materials sciences.* 2013. **113**(18): p. 2110-2142.
18. Sanders, J.M., et al., *Modeling fluid uptake in composite matrix materials using molecular simulation* in *CAMX* 2018: Dallas, TX.
19. Sanders, J.M., et al. *Atomistic modeling of non-epoxy based thermosets: Challenges and prospects* in *CAMX*. 2017. Orlando, FL.